4. R. Lyczak, J. E. Gomes, B. Bowerman, *Dev. Cell* **3**, 157 (2002).
5. J. Pellettieri, G. Seydoux, *Science* **298**, 1946 (2002).
6. A. F. Severson, D. L. Baillie, B. Bowerman, *Curr. Biol.* **12**, 2066 (2002).
7. D. Albertson, *Dev. Biol.* **101**, 61 (1984).
8. S. W. Grill, P. Gönczy, E. H. K. Stelzer, A. A. Hyman, *Nature* **409**, 630 (2001).
9. D. J. Sharp, G. C. Rogers, J. M. Scholey, *Nature* **407**, 41 (2000).
10. P. Gönczy, *Trends Cell Biol.* **12**, 332 (2002).
11. T. J. Mitchison, E. D. Salmon, *Nature Cell Biol.* **3**, E17 (2001).
12. S. C. Schuyler, D. Pellman, *J. Cell Sci.* **114**, 247 (2001).
13. J. Howard, A. A. Hyman, *Nature* **422**, 753 (2003).
14. See supporting data on *Science* Online.
15. M. F. Tsou, W. Ku, A. Hayashi, L. S. Rose, *J. Cell Biol.* **160**, 845 (2003).
16. F. J. Sigworth, *Nature* **270**, 265 (1977).
17. F. J. Sigworth, *J. Physiol. (London)* **307**, 97 (1980).
18. D. Schmidt, S. Strome, unpublished data.
19. D. L. Dujardin, R. B. Vallee, *Curr. Opin. Cell Biol.* **14**, 44 (2002).
20. In the velocity-limited regime, a fragment moves at the maximum velocity whenever there are one or more force generators active. The more force generators per fragment, the higher the mean speed, because the probability of having at least one active force generator is increased. However, this model results in a mean-variance relationship identical to the force-limited case presented, with $N = 1$. This is not consistent with our results.
21. With fewer than 12 aster fragments generated per spindle pole and one or two active force generators per fragment, we expect fewer than 50 active force generators throughout the embryo at any time during anaphase.
22. M. Gotta, J. Ahringer, *Nature Cell Biol.* **3**, 297 (2001).
23. Y. Cai, F. Yu, S. Lin, W. Chia, X. Yang, *Cell* **112**, 51 (2003).
24. P. Gönczy *et al.*, *Nature* **408**, 331 (2000).
25. K. Colombo *et al.*, *Science* **300**, 1957 (2003); published online 15 May 2003 (10.1126/science.1084146).
26. M. Gotta, Y. Dong, Y. K. Peterson, S. M. Lanier, J. Ahringer, *Curr. Biol.* **13**, 1029 (2003).
27. D. G. Srinivasan, R. M. Fisk, H. Xu, S. Van Den Heuvel, *Genes Dev.* **17**, 1225 (2003).
28. E. Hannak *et al.*, *J. Cell Biol.* **157**, 591 (2002).
29. Because the laser was focused at regions where the pericentriolar material and γ-tubulin are localized, we expect a fraction of the centrosomal γ-tubulin to be destroyed. Consequently, not all aster fragments contained detectable levels of γ-tubulin.
30. L. Sachs, *Applied Statistics: A Handbook of Techniques* (Springer, New York, 1984).
31. Stray light from the pulsed ultraviolet (UV) laser used for OICD bleached the surrounding GFP–α-tubulin. Therefore, UV laser power was reduced by about 70% to visualize fragment movement by GFP. With less laser power, we probably produced larger fragments with an increased drag coefficient. Thus, elementary speeds were smaller in the GFP assay than in the DIC assay. On the other hand, larger fragments have more force generators associated, consistent with the general increase in *N* for the GFP assay.

32. We thank C. Cowan, A. Desai, M. Diehl, P. Gönczy, M. Glotzer, E. Hannak, F. Jülicher, K. Oegema, L. Pelletier, A. Riedinger, G. Ritter, E. Sackmann, N. Salmon, M. Srayko, and E. Tanaka for useful discussions, experimental assistance, and helpful comments. Supported by Deutsche Forschungsgemeinschaft grant SPP 1111 (HY3/2-1).

Supporting Online Material

www.sciencemag.org/cgi/content/full/301/5632/518/DC1
Materials and Methods
SOM Text
Figs. S1 to S7
References
Movies S1 to S7

7 May 2003; accepted 18 June 2003

Role of Subplate Neurons in Functional Maturation of Visual Cortical Columns

Patrick O. Kanold, Prakash Kara, R. Clay Reid, Carla J. Shatz*

The subplate forms a transient circuit required for development of connections between the thalamus and the cerebral cortex. When subplate neurons are ablated, ocular dominance columns do not form in the visual cortex despite the robust presence of thalamic axons in layer 4. We show that subplate ablation also prevents formation of orientation columns. Visual responses are weak and poorly tuned to orientation. Furthermore, thalamocortical synaptic transmission fails to strengthen, whereas intracortical synapses are unaffected. Thus, subplate circuits are essential not only for the anatomical segregation of thalamic inputs but also for key steps in synaptic remodeling and maturation needed to establish the functional architecture of visual cortex.

Subplate neurons, located in the developing white matter (WM), are among the first postmitotic cortical neurons (*1*). They are also first to receive functional synaptic inputs from the thalamus; their axons relay this input into the cortical plate well in advance of the invasion of thalamic axons into layer 4 (*1*). Once thalamic axons have arrived in layer 4, subplate neurons are gradually eliminated during the period of ocular dominance column (ODC) formation (*1*–*3*). Thus, subplate neurons are in a key, intermediate position to control the flow of information into the developing cortex when first spontaneous (prenatal) and then visual (postnatal) activity are present (*3*). Early subplate ablation prevents the invasion of thalamic axons into layer 4 (*4*), whereas later ablation blocks the anatomical segregation of thalamic axons from the lateral geniculate nucleus (LGN) into ODCs in primary visual cortex (*5*).

The prevailing hypothesis about ODC formation and plasticity is that activity-dependent competition between LGN axons representing each eye leads to their selective growth or pruning (*3*). However, recent observations that ODCs emerge earlier than previously thought, even before the onset of patterned visual experience (*2*, *6*), have required a revision of this hypothesis, and one suggestion is that subplate neurons are involved (*2*).

To determine how the subplate might influence functional development and organization of visual cortex, subplate neurons were selectively ablated at P6 to P9 in cats (*7*). This time is just before the onset of ODC formation (*6*, *8*, *9*) and just after the ingrowth of LGN axons to cortical layer 4 (*10*). To make localized and selective ablations, we either used kainic acid injections (*4*, *5*) or an immunotoxin (*11*, *12*) to p75, a neurotrophin receptor expressed in the neocortex only by subplate neurons at this age (*1*).

Response properties of cortical neurons were evaluated after subplate ablation by optical imaging and microelectrode recordings at P24 to P49 (*7*), when well-organized orientation maps are normally present (*6*, *13*, *14*). Orientation maps in control hemispheres or far from the ablation were highly organized (Fig. 1A, left and center), in contrast to poor organization in the highly local region surrounding the immunotoxin-ablated area (Fig. 1A, center). Kainic acid injections created even larger regions of disrupted or absent orientation maps (Fig. 1A, right). Polar maps representing both the angle and strength of tuning revealed weaker orientation selectivity in the ablated region (Fig. 1B), indicating the existence of an additional severe functional deficit. ODC maps were also degraded in ablated hemispheres (fig. S1), consistent with previous anatomical data (*5*).

Degraded orientation maps can result from neurons well tuned to different orientations but not segregated into columns, from neurons poorly tuned for orientation, or simply from neurons that respond poorly to visual stimuli. To distinguish between these alternatives, ocular dominance and orientation tuning of single cortical neurons were measured with microelectrode recordings (*7*) in both ablated and control regions in each animal (Fig. 1A and fig. S2). Because LGN axons are abundant in layer 4 of subplate-ablated cortex (Fig. 2A) (*5*), we had expected to find strong visually driven responses. Instead, there were fewer visually responsive units in the ablated area (*15*), and they were less orientation-selec-

Department of Neurobiology, Harvard Medical School, Boston, MA 02115, USA.

*To whom correspondence should be addressed. E-mail: carla_shatz@hms.harvard.edu

tive (Fig. 1, C and D). In addition, visually driven units in ablated cortex were only weakly driven by the ipsilateral eye, resulting in a strong response bias toward the contralateral eye (*15*). This bias is reminiscent of normal visual cortex at earlier developmental ages (*6*, *13*), suggesting arrested development.

Alterations in cortical organization, as measured by several anatomical and molecular correlates, were also similar after immunotoxin or kainate ablations. In the immunotoxin-ablated region, uniform transneuronal labeling showed that ODCs were absent despite a robust projection from the LGN to layer 4 (Fig. 2A), as with kainate ablations (*5*); ODCs were present in immediately adjacent unablated regions. Brain-derived neurotrophic factor (BDNF) mRNA (*7*) also increased in layers 2 to 4 of cortex located above the immunotoxin-ablated region (Fig. 2, B and D), as occurs after kainate ablations (*16*).

Although immunotoxin ablation altered geniculocortical connectivity, gene expression, and columnar functional organization of cortex, the gross histology of cortical layers residing above the ablation site was indistinguishable from that of unablated adjacent regions (Fig. 2E). Cortical p75 is almost exclusively restricted to the subplate (*1*), but cholinergic fibers from basal forebrain are also known to express p75 (*17*). Therefore, we also verified that cholinergic fibers were abundant in immunotoxin-ablated regions (fig. S4). The only obvious histological effect seen after immunotoxin injection was the loss of neurons in WM, as expected because subplate neurons are normally located there (Fig. 2, F and G).

In summary, both immunotoxin and kainate treatments have similar consequences for cortical development yet act through completely different mechanisms. Thus, observed changes are specifically because of removal of subplate neurons rather than nonspecific effects of the injections (*18*).

One explanation for the functional deficits in visual cortex is that LGN neurons are affected by subplate ablation. When we recorded in the LGN, however, neurons projecting to the ablated site had responses and receptive field organization (Fig. 3A) appropriate for this age (*19*). Thus, observed defects in orientation tuning and visual responsiveness must occur beyond the LGN.

To examine whether the cortical defect originates at thalamocortical synapses, we electrically stimulated the LGN while we recorded evoked field potentials at a retinotopically matching cortical location in vivo. Field potentials in subplate-ablated regions were smaller in all layers, particularly layer 4, than those in control regions (Fig. 3B), consistent with only weak activation of thalamocortical synapses. These results were confirmed by in vitro recordings from slices of visual cortex (*7*). Field potentials recorded in layers 2/3 and 4, evoked by WM stimulation, were vastly reduced in the ablated regions (Fig. 3C). The size of the monosynaptic response in layer 4 was significantly smaller, implying very weak thalamocortical synapses (Fig. 3D). In contrast, evoked potentials in layer 2/3 after layer 4 stimulation were close to normal in amplitude and waveform in ablated regions (Fig. 3E).

Histological observations and in vivo recordings indicate that layer 4 neurons are present after subplate ablation. Whole-cell patch recordings performed on layer 4 neurons in slices (*8*) confirmed that neurons from ablated regions fired action potentials to current injections (Fig. 4A), had normal measures of intrinsic membrane properties (Fig. 4B), and appeared to have normal dendritic morphology (Fig. 4A, inset). The attenuated field potentials after subplate ablation could reflect a lack of spatial organization and neuronal synchrony in subplate-ablated cortex or an underlying attenuation of synaptic currents. Direct measurement of the size of excitatory synaptic inputs to layer 4 neurons showed that excitatory postsynaptic currents evoked by electrical WM stimulation (eEPSCs) were reduced by 80% in subplate-ablated slices compared to those of controls (Fig. 4C; see also fig. S5).

Because thalamocortical axons are present in layer 4 (for example, Fig. 2A) and LGN neurons have normal visual responses, it is possible that the attenuation in thalamocortical transmission is because of a postsynaptic defect. In fact, mRNA expression of the dominant AMPA receptor subunit, GluR1, is selectively reduced by 65% within layer 4 in the ablated area (Fig. 4D), implying that the maturation of layer 4

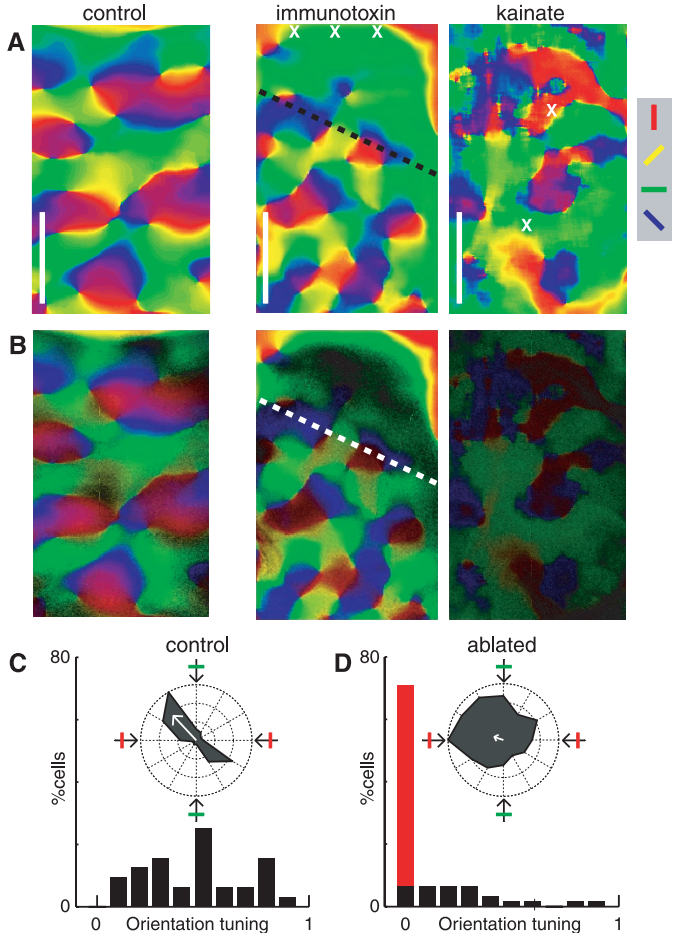

Fig. 1. Subplate ablation disrupts orientation maps and prevents sharpening of orientation tuning. (**A**) In vivo optical imaging of orientation maps in control and ablated visual cortex. Color indicates preferred orientation at each pixel. Scale bars indicate 1 mm. Each immunotoxin or kainate injection site is marked with an "x." Compared with control hemisphere (left), which shows robust orientation domains and pinwheels, maps in subplate-ablated hemispheres at P48 after immunotoxin injections at P8 and at P37 after kainate at P9 are disorganized in regions receiving ablations. Immunotoxin treatments ($n = 2$ animals) are more focal (area above dashed line) than with kainate ($n = 5$ animals). Optical maps after sham injections (saline) were indistinguishable from that of the control [$n = 1$ animal (*29*)]. (**B**) Polar maps showing both preferred orientation (color) and tuning strength (brightness). Strong orientation-selective responses (bright colors) and pinwheels are evident in unablated areas. Orientation maps are nonselective (dark) and unorganized in ablated cortex. (**C** and **D**) Summary histograms of orientation-tuning strength (OTS) (*7*) of single units in ablated (C) and control (D) cortex (0, unselective; 1, perfectly selective). Compared to control (0.48 ± 0.25, $n = 31$), OTSs of all units (including unresponsive units, in red) were reduced by 82% in ablated cortex (0.09 ± 0.15, $n = 62$, $P < 0.00001$). Compared to those of controls (0.48 ± 0.25, $n = 31$), OTSs in ablated cortex of just the visually driven units (black) were reduced by 44% (0.27 ± 0.24, $n = 22$, $P < 0.005$). Insets show typical OTS examples.

synapses is impaired. In marked contrast to the decreased eEPSC amplitudes after subplate ablation (Fig. 4C), the amplitudes of the spontaneous miniature EPSCs (mEPSCs) are unchanged in layer 4 neurons (Fig. 4E), and their frequency actually increased (Fig. 4F). The observed increase in spontaneous activity in the face of decreased thalamic inputs is consistent with the presence of a homeostatic mechanism controlling overall synaptic input (*20*). Taken together, recordings from layer 4 in vivo and in vitro indicate that layer 4 neurons are present and can receive intracortical synaptic input (as evident from the mEPSCs) but that there has been a selective loss of synaptic drive from the thalamus.

The major finding of this study is that subplate ablation leads to an impairment in synaptic transmission of visually driven activity from the LGN into cortical circuits. Although LGN axons are present in layer 4, the cortex becomes essentially uncoupled from the thalamus, as assessed both in vivo and in vitro. In addition, functional ODCs and orientation maps do not develop [Supporting Online Material (SOM) Text]. Although the majority of neurons were unresponsive to visual stimuli, some cells did have robust visual responses but nevertheless were not orientation-selective. This global absence of functional tuning of cortical maps after subplate ablation is related to the failure of thalamocortical synapses to strengthen and the abnormally low expression in layer 4 neurons of key molecular components mediating glutamatergic transmission, such as GluR1.

How can subplate ablation lead to the observed functional decoupling of thalamus from cortex? Although increased feed forward inhibition could mask thalamocortical EPSCs, our observation of increased mEPSC frequency and absence of large inhibitory postsynaptic currents makes this hypothesis unlikely. We favor the hypothesis that depolarizing input from subplate

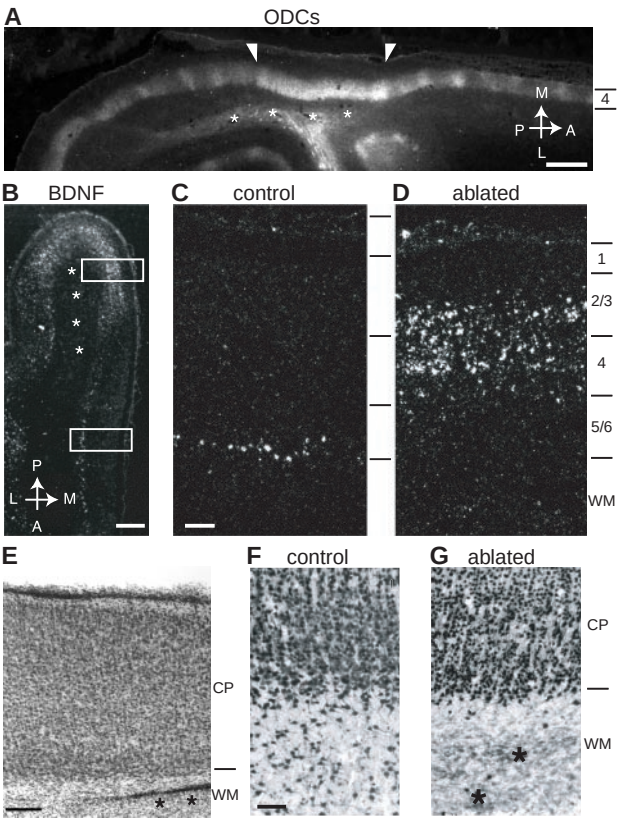

Fig. 2. Immunotoxin ablation of subplate neurons prevents segregation of LGN axons into ODCs and upregulates expression of BDNF in cortex. (**A**) Darkfield autoradiograph of visual cortex at P82 after four injections (indicated by asterisks) of immunotoxin at P9 (two posterior injections of 0.25 mg/ml and two anterior injections of 0.5 mg/ml). ODCs were visualized by transneuronal transport after monocular injection of ^{3}H-proline (*7*). (Silver grains, which label LGN axons and axon terminals, appear white in darkfield autoradiograph.) Ablation extended ~1 mm from each injection site, consistent with reported data (*11*). Robust, continuous transneuronal labeling (between arrowheads) in layer 4 signifies absence of ODCs above the subplate ablation zone as compared to patchy labeling of ODCs in control regions. Control immunotoxin treatment does not disrupt ODCs (fig. S3). (**B**) In situ hybridization (darkfield autoradiograph) shows increased BDNF mRNA expression in cortex at P16 after four immunotoxin (1 mg/ml) injections (asterisks) into subplate at P9. Boxes indicate locations of (C) and (D). (**C** and **D**) BDNF mRNA is abnormally increased in layers 2/3 and 4 in subplate-ablated (D) but not adjacent control (C) cortex. Normally, at this early age, BDNF mRNA expression is restricted to the subplate–layer 6 border (*30*). Cortical layers and WM indicated on right. (**E**) Histology of cortical plate (CP) at P28 (cresyl stain) appears normal after immunotoxin (1 mg/ml) ablations at P7. The presence of fluorescent microspheres (coinjected with immunotoxin) in the WM is indicated (above asterisks). (**F** and **G**) Immunohistochemistry with the use of NeuN [a neuron-specific marker (Chemicon, Temecula, CA)] confirms selective loss of subplate neurons at injection sites [indicated by asterisks in (G)]. Scale bars, 1 mm [(A) and (B)], 0.2 mm [(C), (D), and (E)], and 80 μm [(F) and (G)].

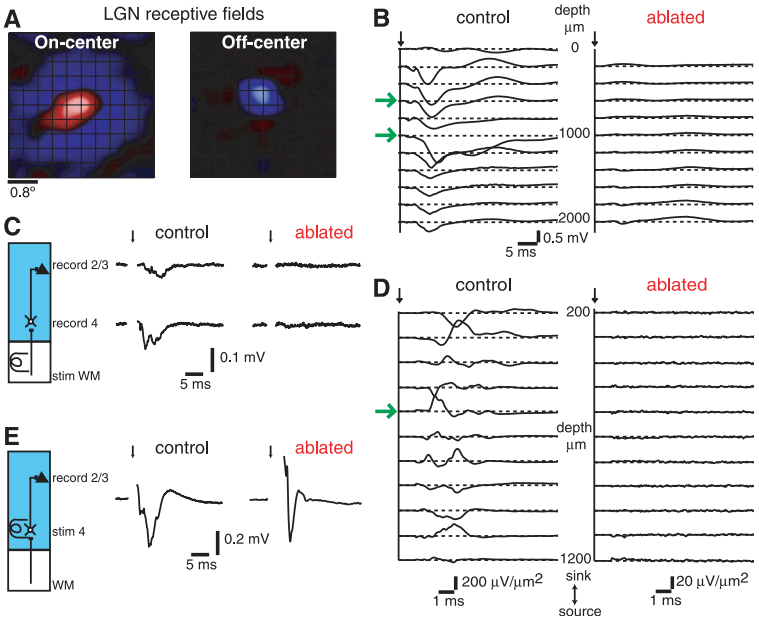

Fig. 3. Subplate ablation alters thalamocortical but not intracortical field potentials. (**A**) Typical LGN receptive fields (P48) that retinotopically overlapped the visual cortex receiving immunotoxin ablations at P8. Receptive-field size and organization are within normal range for these ages (*19*). (**B**) In vivo cortical field potentials after electrical stimulation of LGN at matching retinotopic locations (vertical arrows mark stimulus onset). Fields are smaller in ablated compared with control regions throughout all layers (layer 4 is between green arrows). (**C**) Field recordings in vitro from ablated versus control hemispheres in cortical slices at P30 (ablated at P8) (*7*). WM stimulation evokes large field potentials in layer 2/3 and layer 4 in control slices (n = 16), whereas only small field potentials are present in these layers in ablated slices (n = 24). Stimulus artifacts are removed. (**D**) First-order current-source density (CSD) calculated from field potentials recorded in slices after WM stimulation. In control slices (left), a large monosynaptic sink is present at ~1.5-ms latency in layer 4 (green arrow). Large, longer latency sinks are visible in layers 2/3 and 5/6. In contrast, no layer 4 sinks are present in ablated hemispheres (right) (CSD variance of 820 ± 1600 $\mu V^2/mm^4$ versus 3.4 ± 2.5 $\mu V^2/mm^4$, $P < 0.002$, Mann-Whitney). (**E**) Electrical stimulation of layer 4 in slices from ablated or control hemispheres produces monosynaptic field potentials in layer 2/3, demonstrating intact transmission from layer 4 to layer 2/3 even in ablated regions (n = 15).

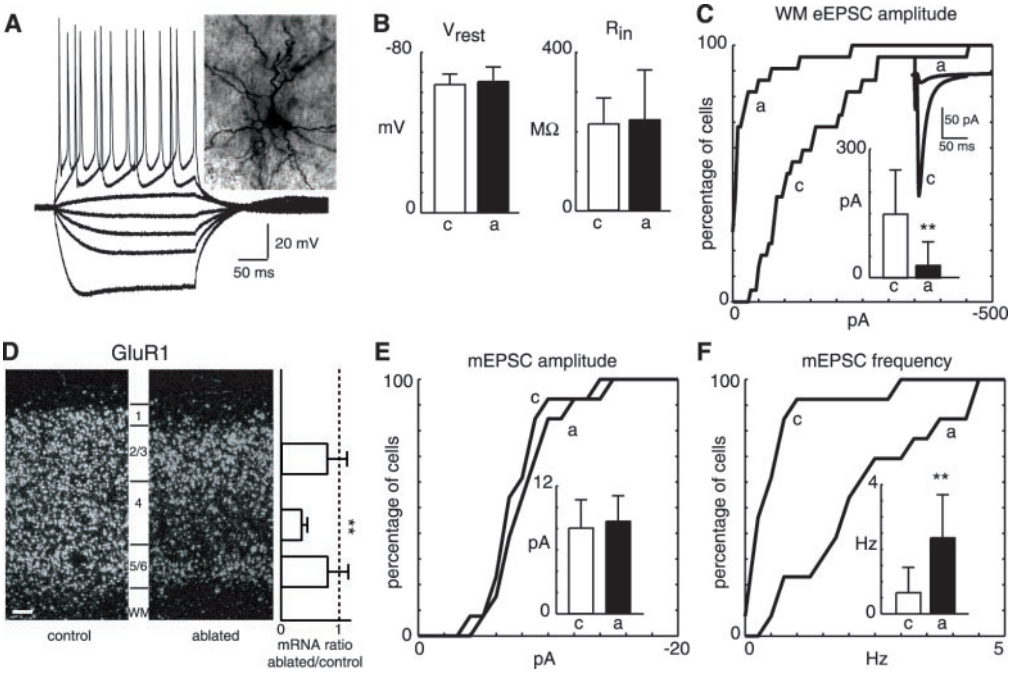

Fig. 4. Subplate ablation alters thalamocortical synaptic efficacy in layer 4 neurons. (**A**) Whole-cell recording of a layer 4 neuron in a subplate-ablated cortical slice (*7*). Traces show responses to multiple current injections. Inset shows a biocytin-filled layer 4 neuron with normal morphology located in ablated region. (**B**) Neurons from control ("c") as compared to ablated ("a") slices have similar resting potential (−63.9 ± 5.2 mV for control, n = 24, as compared to −65.4 ± 7.3 mV for ablated, n = 20; $P > 0.1$) and input resistance (217.8 ± 65.4 MΩ for control, n = 24, as compared to 225.3 ± 125.9 MΩ for ablated, n = 20; $P > 0.1$). (**C**) Cumulative amplitude histograms show that WM stimulation evokes eEPSCs in ablated or control slices. The eEPSC amplitude (inset) is 80% smaller in ablated slices (29.3 ± 54.6 pA for ablated, n = 22, as compared to 148.3 ± 102.9 pA for control, n = 22; $P < 0.0001$, double asterisks). Adjacent traces show mean eEPSCs of representative neurons from each population. eEPSC amplitudes from saline and control-immunotoxin slices are indistinguishable from control (fig. S5). (**D**) Darkfield autoradiograph of in situ hybridization for GluR1 mRNA in control (left) or ablated (right) cortex. Scale bar, 0.2 mm. Densitometry (histogram) shows that layer 4 GluR1 mRNA levels in ablated regions are reduced to 35% of that of controls ($P < 0.005$, double asterisks, n = 4 animals). GluR1 mRNA levels are unchanged after layer 4 kainate injections (n = 2 animals) (fig. S6) or saline injections into the subplate [n = 1 animal (*29*)]. (**E**) Cumulative histograms and bar graphs (inset) show that mEPSC amplitudes are similar (8.6 ± 2.4 pA for ablated, n = 13, compared to 8.0 ± 2.6 pA for control, n = 13; $P > 0.1$). (**F**) Cumulative mEPSC frequency histograms and bar graph (inset) show that mEPSC frequency is 3.6-fold higher in ablated slices (2.34 ± 1.34 Hz for ablated, n = 13, compared to 0.65 ± 0.08 Hz for control, n = 13; $P < 0.001$, double asterisks).

neurons is needed for the activation of previously "silent" thalamocortical synapses (*21*) because subplate neurons supply excitatory input to cortical neurons (*22*, *23*). In this case, some form of learning rule, known to be present at thalamocortical synapses (*24*, *25*), is disrupted in the absence of subplate neurons, preventing the progressive strengthening of thalamic synapses. The observation here that GluR1 mRNA is decreased after subplate ablation implies that excitatory drive on all cortical neurons, including inhibitory neurons, is also diminished.

It is remarkable that eye segregation fails even though LGN receptive fields are normal and both LGN axons and layer 4 neurons are present in subplate-ablated cortex. Our observations constrain mechanisms of patterning of connectivity in cortical circuits. It has been suggested that thalamocortical connectivity during the critical period depends on cortical circuits outside of layer 4 (*26*). In contrast, our findings show that patterning of thalamocortical connectivity before onset of the critical period crucially depends on proper LGN input to the cortex, as regulated by subplate neurons. Furthermore, Crowley and Katz have proposed that eye-specific molecular cues set up the initial pattern of ODCs during development (*2*, *27*), with activity being required only at later ages. If so, then our results argue that these hypothetical molecular cues in cortex reside not in layer 4 or LGN axon terminals, both of which are present in the subplate-ablated cortex, but instead in the subplate. Alternatively, subplate neurons could mediate very early activity-dependent interactions driven by correlated spontaneous activity relayed from the retina to the cortex by LGN neurons, which is also known to be present in corticogeniculate circuits (*3*, *28*). Regardless of which alternative proves to be the case, our observations here demonstrate that circuits formed by subplate neurons are needed both for strengthening and for selective remodeling of thalamocortical excitatory synaptic connections that underlie the development of columnar organization in cortex.

References and Notes

1. K. L. Allendoerfer, C. J. Shatz, *Annu. Rev. Neurosci.* **17**, 185 (1994).
2. J. C. Crowley, L. C. Katz, *Science* **290**, 1321 (2000).
3. L. C. Katz, C. J. Shatz, *Science* **274**, 1133 (1996).
4. A. Ghosh, A. Antonini, S. K. McConnell, C. J. Shatz, *Nature* **347**, 179 (1990).
5. A. Ghosh, C. J. Shatz, *Science* **255**, 1441 (1992).
6. M. C. Crair, J. C. Horton, A. Antonini, M. P. Stryker, *J. Comp. Neurol.* **430**, 235 (2001).
7. Materials and methods are available as supporting material on *Science* Online.
8. In cats, ODCs form at about P14 (*6*) or later. Moreover, even at P19, many individual axons have broadly distributed processes that have not yet focused their branching to the width of an ODC (*9*).
9. A. Antonini, M. P. Stryker, *J. Neurosci.* **13**, 3549 (1993).
10. C. J. Shatz, M. B. Luskin, *J. Neurosci.* **6**, 3655 (1986).
11. L. Mrzljak, A. I. Levey, S. Belcher, P. S. Goldman-Rakic, *J. Comp. Neurol.* **390**, 112 (1998).
12. A. Fine *et al.*, *Neuroscience* **81**, 331 (1997).
13. M. C. Crair, D. C. Gillespie, M. P. Stryker, *Science* **279**, 566 (1998).
14. B. Chapman, M. P. Stryker, T. Bonhoeffer, *J. Neurosci.* **16**, 6443 (1996).
15. Many neurons in ablated regions were not well driven by visual stimuli [average responsiveness (AR) = 1.02 ± 1.1; 36 of 86 units were unresponsive and only 13 of 86 units were strongly driven], whereas neurons outside poorly tuned regions were strongly responsive to visual stimuli (AR = 2.65 ± 0.67; 2 of 59 units were unresponsive and 43 of 59 units were strongly driven; $P < 0.0001$). Neurons in ablated areas showed increased spontaneous firing rate (a control rate of 0.66 ± 0.9 Hz as compared to an ablated rate of 2.6 ± 4.4 Hz, $P < 0.07$), whereas visually driven rates were similar (a control rate of 4.3 ± 3.5 Hz compared with an ablated rate of 7.4 ± 9.2 Hz, $P > 0.5$). Visual responsiveness (VR) to ipsilateral eye stimulation is smaller in neurons from ablated regions ($VR_{control}$ = 2.54 ± 1.91, n = 31; $VR_{ablated}$ = 0.85 ± 0.95, n = 19; $P < 0.0001$). VR to contralateral eye stimulation was similar ($VR_{control}$ = 2.12 ± 1.84, n = 31; $VR_{ablated}$ = 2.02 ± 1.67, n = 15; $P > 0.1$), resulting in response bias toward the contralateral eye for neurons in ablated regions but not control regions as measured by the Contralateral Bias Index (CBI) ($CBI_{ablated}$ = 0.48 ± 0.62, $CBI_{control}$ = −0.1 ± 0.39, $P < 0.005$).
16. E. S. Lein, E. M. Finney, P. S. McQuillen, C. J. Shatz, *Proc. Natl. Acad. Sci. U.S.A.* **96**, 13491 (1999).
17. E. P. Pioro, A. C. Cuello, *Neuroscience* **34**, 57 (1990).
18. Nonspecific inflammation after injections also cannot account for observed changes because control

immunotoxin (saporin linked to a nonspecific mouse immunoglobulin G) injections, saline injections into subplate, and kainate injections into layer 4 have no effect on ODCs (*5*, *16*) (fig. S3). Furthermore, control immunotoxin and saline injections do not alter synaptic physiology as assessed in slices (fig. S5). Layer 4 injections of kainate or saline injections into subplate, although right at the site of the disconnection effects and causing mechanical damage from the injection needle, do not disrupt any known aspect of cortical structure or gene expression that have been monitored (*5*, *16*) (fig. S6).

19. D. Cai, G. C. DeAngelis, R. D. Freeman, *J. Neurophysiol.* **78**, 1045 (1997).
20. G. G. Turrigiano, S. B. Nelson, *Curr. Opin. Neurobiol.* **10**, 358 (2000).
21. J. T. Isaac, M. C. Crair, R. A. Nicoll, R. C. Malenka, *Neuron* **18**, 269 (1997).
22. E. M. Finney, J. R. Stone, C. J. Shatz, *J. Comp. Neurol.* **398**, 105 (1998).
23. E. Friauf, C. J. Shatz, *J. Neurophysiol.* **66**, 2059 (1991).
24. M. C. Crair, R. C. Malenka, *Nature* **375**, 325 (1995).
25. D. E. Feldman, R. A. Nicoll, R. C. Malenka, J. T. Isaac, *Neuron* **21**, 347 (1998).
26. J. T. Trachtenberg, C. Trepel, M. P. Stryker, *Science* **287**, 2029 (2000).
27. J. C. Crowley, L. C. Katz, *Nature Neurosci.* **2**, 1125 (1999).
28. M. Weliky, L. C. Katz, *Science* **285**, 599 (1999).
29. P. O. Kanold, P. Kara, R. C. Reid, C. J. Shatz, unpublished data.
30. E. S. Lein, A. Hohn, C. J. Shatz, *J. Comp. Neurol.* **420**, 1 (2000).
31. We thank R. Born for helpful discussions; M. Marcotrigiano, B. Printseva, and S. Yurgensen for surgical, histological, and technical assistance; and D. Butts, M. Majdan, J. Syken, and Y. Tagawa for helpful comments on the manuscript. Supported by NIH R01 EY02858 (C.J.S.), F32 EY1352 (P.O.K.), R01 EY10115 (R.C.R.), and P30 EY12196 (R.C.R.).

Supporting Online Material

www.sciencemag.org/cgi/content/full/301/5632/521/DC1
Materials and Methods
SOM Text
Figs. S1 to S6

4 March 2003; accepted 13 June 2003

Melanopsin Is Required for Non–Image-Forming Photic Responses in Blind Mice

Satchidananda Panda,[1,2]* Ignacio Provencio,[4]* Daniel C. Tu,[5]* Susana S. Pires,[1] Mark D. Rollag,[4] Ana Maria Castrucci,[4,7] Mathew T. Pletcher,[1,2] Trey K. Sato,[1,2] Tim Wiltshire,[1] Mary Andahazy,[1] Steve A. Kay,[2] Russell N. Van Gelder,[5,6] John B. Hogenesch[1,3]†

Although mice lacking rod and cone photoreceptors are blind, they retain many eye-mediated responses to light, possibly through photosensitive retinal ganglion cells. These cells express melanopsin, a photopigment that confers this photosensitivity. Mice lacking melanopsin still retain nonvisual photoreception, suggesting that rods and cones could operate in this capacity. We observed that mice with both outer-retinal degeneration and a deficiency in melanopsin exhibited complete loss of photoentrainment of the circadian oscillator, pupillary light responses, photic suppression of arylalkylamine-*N*-acetyltransferase transcript, and acute suppression of locomotor activity by light. This indicates the importance of both nonvisual and classical visual photoreceptor systems for nonvisual photic responses in mammals.

The eye is the principal mediator of light input to the central nervous system in mammals. In addition to vision, the eye mediates several nonvisual responses to light, including photoentrainment of the circadian oscillator, constriction of the pupil, acute suppression of pineal melatonin, acute suppression of activity (masking) in nocturnal mammals, and regulation of sleep latency. Many of these responses persist in mice that are visually blind from outer-retinal degeneration but are abolished by bilateral enucleation of the eyes (*1*). Here, we demonstrate the presence of inner-retinal, nonvisual ocular photoreceptors that specifically subserve these nonvisual photic responses.

Intrinsically photosensitive retinal ganglion cells (ipRGCs) (*2*, *3*) project to brain sites that mediate many of these ocular, yet nonvisual, responses to light, including the suprachiasmatic nucleus (SCN), the intergeniculate leaflet, and the olivary pretectal nucleus, which mediates pupillary light reflexes (PLR) (*1*). The photosensitivity of these cells ex vivo depends on the presence of melanopsin (Opn4), a member of the opsin family of photopigment proteins (*4*). Whereas melanopsin-deficient (*Opn4*$^{-/-}$) mice exhibit moderate attenuation in light-induced phase resetting of the circadian oscillator (*5*, *6*) and reduced PLR under high irradiance levels (*4*), most nonvisual photic responses in these mice remain largely intact. This suggests either the presence of additional inner-retinal photoreceptors, or contributions from the outer-retinal classical photoreceptors to nonvisual photoresponses. To test the latter hypothesis, we generated mice that were deficient in both melanopsin and classical photoreceptors by breeding *Opn4*$^{-/-}$ mice (*5*) with the C3H/HeJ mouse strain that carries the retinal degeneration (*rd*) mutation (*7*). Mice homozygous for the *rd* allele are visually blind as a result of a primary degeneration of the rods and a secondary loss of cones, but they retain melanopsin-containing RGCs (fig. S1). The *Opn4*$^{-/-}$; *rd*/*rd* mice were healthy and viable with intact optic nerves. Outer retinal degeneration was indistinguishable between *rd*/*rd* and *Opn4*$^{-/-}$; *rd*/*rd* mice (fig. S1).

To assess the circadian photoentrainment and acute light suppression of activity, we subjected the *Opn4*$^{-/-}$; *rd*/*rd* mice, littermate wild-type, *rd*/*rd*, and *Opn4*$^{-/-}$ mice to a 24-hour light:dark (LD) cycle (8L:16D) (*7*). Under conditions of constant darkness (DD), mice have a free-running circadian locomotor period of less than 24 hours. However, in a 24-hour LD cycle, photic input to the oscillator makes a small phase adjustment in each cycle and synchronizes the clock to an exact 24-hour period (photoentrainment). Wild-type mice and the single *Opn4*$^{-/-}$ and *rd*/*rd* mutants entrained normally and consolidated their wheel-running activity to the dark period of the LD cycle (Fig. 1) as has been previously reported (*5*, *6*, *8*). In contrast, the *Opn4*$^{-/-}$; *rd*/*rd* mice failed to entrain to the external lighting cycle and continued to exhibit free-running rhythms (Fig. 1 and Table 1). In addition, increasing the light intensity to 800 lux during the photoperiod and increasing the photoperiod to 12 hours failed to entrain these mice (Fig. 1 and Table 1; fig. S2).

All four genotypes exhibited free-running DD periods of <24 hours (Table 1). Under constant light (LL) conditions, most nocturnal

[1]Genomics Institute of the Novartis Research Foundation, 10675 John J. Hopkins Drive, San Diego, CA 92121, USA. [2]Department of Cell Biology, [3]Department of Neuropharmacology, Scripps Research Institute, 10550 North Torrey Pines Road, San Diego, CA 92037, USA. [4]Department of Anatomy, Physiology, and Genetics, Uniformed Services University, 4301 Jones Bridge Road, Bethesda, MD 20814, USA. [5]Department of Ophthalmology and Visual Sciences, [6]Department of Molecular Biology and Pharmacology, Washington University School of Medicine, 660 South Euclid Avenue, St. Louis, MO 63110, USA. [7]Department of Physiology, Biosciences Institute, University of São Paulo, Rua do Matão, travessa 14, 05508-900, São Paulo, Brazil.

*These authors contributed equally to this work.
†To whom correspondence should be addressed. E-mail: hogenesch@gnf.org